Fabrication of large-area fully alloyed Ag/Au

nanoparticle arrays

Oludare E. Babawale<sup>†</sup> and Lars Gundlach\*,†,‡

†Department of Chemistry and Biochemistry, University of Delaware, Newark, DE 19716,

USA

Department of Physics and Astronomy, University of Delaware, Newark, DE 19716, USA

E-mail: larsg@udel.edu

Abstract

The potential applications of nanoparticles in future technologies are extensive.

Many of those applications require assembly of mono-dispersed nanostructures into

ordered macroscopic building blocks, such as arrays, to enable their integration into

complex devices. Examples of such applications include electrical contacts to nanopar-

ticles in electro-optical devices and nano-gap-enabled chemical sensors.

Herein, we present a versatile approach to fabricate extended and highly ordered

arrays of fully alloyed Ag/Au nanoparticles on solid substrates that can easily be ex-

panded to other binary and even higher alloys. The strategy is demonstrated by fab-

ricating Ag/Au alloys with Ag compositions ranging from 0% to 100%. As expected,

the plasmon resonance of the alloyed nanoparticles could be varied between those of

pristine Au and Ag. The width of the plasmon resonance was significantly smaller

compared to partially low-temperature alloyed mixtures presented previously. Finally,

a Cu<sub>2</sub>O semiconductor shell was grown on the alloy core to demonstrate that the re-

sulting nanoparticle surfaces are accessible for functionalization, therefore broadening

the potential applications of the material.

1

Keywords: Alloy Nanoparticles, Localized Surface Plasmon, Ordered Nanoparticle Structures, Nanosphere Lithography, Metal/Semiconductor Hybrids

#### INTRODUCTION

Ordered nanoparticle structures such as 2D arrays are essential for integrating large numbers of nanoparticles into complex devices and to address single nanoparticles. Post-synthetic assembly of nanoparticles frequently relies on solution-phase synthesis; however, this process is known to be limited by size and composition inhomogeneity. Also, it often involves surfactants and capping agents for stabilization which are problematic in many applications. <sup>1,2</sup>

Among the vast variety of nanoparticles, metal nanoparticles play an important role in many scientific fields such as catalysis, biochemistry & biopharmaceutical science, optics, and plasmonics. Many recent advancements in the field of plasmonics can be attributed to the development of nanostructures that possess novel properties and functionalities. Noble metals are a major focus of these advancements due to their chemical resistivity and prominent localized surface plasmon resonances (LSPRs).<sup>3</sup> LSPRs can be exploited in a wide range of potential applications including solar energy conversion, photodetection, optoelectronics, photovoltaics, photocatalysis, enhanced spectroscopy, plasmonic imaging, and biotechnology. 4-9 Au and Ag nanoparticles have been broadly investigated because their LSPR is located in the visible spectral range which makes them compatible with many optical technologies. 10 Furthermore, the fabrication of Au and Ag nanoparticles is well established and widely published. Numerous investigations have explored the control of the LSPR by varying parameters such as size, shape, and dielectric environment. 11-17 Controlling the composition of alloyed metal nanoparticles can greatly expand the possibilities for adjusting their properties and can lead to entirely new functionalities. 18 Alloys can combine properties exclusive to the individual metal nanoparticle components, and novel properties due to the synergistic effects of the individual components. However, fabricating homogeneously alloyed nanoparticles is complicated by their large surface-to-volume ratio leading to preferential sublimation and reactions at the surface. 18,19

Binary alloys comprising Ag and Au are among the most reported in literature, <sup>12,13,18,20–23</sup> because their alloy formation is thermodynamically and kinetically favorable on the nanoscale. <sup>3,24–27</sup> The large extinction cross-section and narrow LSPR line width within the visible range make Ag nanoparticles advantageous for many applications. <sup>3,11,19,28,29</sup> However, the application of pure Ag is restricted by its poor stability against chemical, thermal, and oxidative factors. <sup>3,11,19,29</sup> On the other hand, Au has better stability, biocompatibility, and resistance to oxidation. <sup>17</sup> Alloying these two metals in nanoparticles can enable the development of complementary properties. <sup>19</sup> For example, alloying enables tuning of the LSPR frequency while maintaining a constant nanoparticle shape and size. <sup>19,30</sup> Plasmonic applications in particular require complete homogeneous alloying of the constituents to prevent weakening and broadening of the plasmon resonance. <sup>3</sup> However, complete alloying can only be achieved at elevated temperatures that lead to preferential sublimation of silver.

A range of different methods for the synthesis of Ag/Au alloy nanoparticles in suspension have been reported and they include photochemical co-reduction of Au & Ag salts, <sup>31</sup> laser alloying, <sup>32,33</sup> laser ablation of Au & Ag alloy targets <sup>34</sup> and seeded growth synthesis. <sup>17</sup> To enable uniformity and reduce agglomeration of colloidal nanoparticles, wet chemistry methods often rely on electrostatic or steric stabilization. This process involves utilizing capping agents which can limit plasmonic response and introduces additional complexity to the system. <sup>35,36</sup> In addition, inhomogeneities of nanoparticles in suspension often complicate accurate characterization. <sup>10</sup> Full alloying of Ag@Au core/shell nanoparticles from solution-based synthesis has been reported, however, the achievable ratio was limited to Ag-rich particles. <sup>19</sup>

Direct fabrication of thermally alloyed Au/Ag nanoparticles on substrates, on the other hand, has proven to be difficult due to the low stability of Ag and evaporation during the alloying process. Lithographic techniques such as electron beam lithography and focused ion

beam have been employed for fabricating highly ordered 2D arrays. In particular, nanosphere lithography (NSL) has shown to be an effective technique for producing large well-ordered arrays. 37-39 However, most studies on NSL were focused on either fabricating nanostructures from different materials such as halides or with different morphologies. 40-42 While mixedphase metal nanoparticle arrays have been reported, 43 to the best of our knowledge, there has been no report on the fabrication of an ordered array of fully alloyed Ag/Au nanoparticles on a solid substrate using NSL technique. In this work, NSL technique is combined with physical vapor deposition (PVD) to fabricate an extended regular array of fully alloyed Ag/Au hemispherical nanoparticles on solid substrates. The mixed metal particles were protected by a silica shell during high-temperature annealing to achieve complete alloying. 13,19,24 PVD and wet chemistry techniques for capping the particles were compared. The silica cap maintains the hemispherical shape of the alloy following atomic re-distribution at elevated temperatures.<sup>24</sup> The silica capping layer can be fully removed by etching, allowing further functionalization of the alloy nanoparticle. This has been demonstrated by adding a cuprous oxide (Cu<sub>2</sub>O) shell around the alloyed nanoparticles using chemical bath deposition (CBD). It should be mentioned that the technique presented here can easily be modified to include different metals and it can be expanded to include higher alloys.

### **EXPERIMENTAL**

#### Materials

The substrates utilized for the experiments are fused silica and microscope glass cover slides purchased from Advalue Technology and Fisher Scientific, respectively. Polystyrene microspheres employed as masks were obtained from Polysciences Inc. Toluene, sodium dodecyl sulfate, and sodium citrate solution were sourced from Fisher scientific. Finally, hydroxylamine hydroxide and copper(II) sulfate pentahydrate solution were acquired from Sigma-Aldrich.

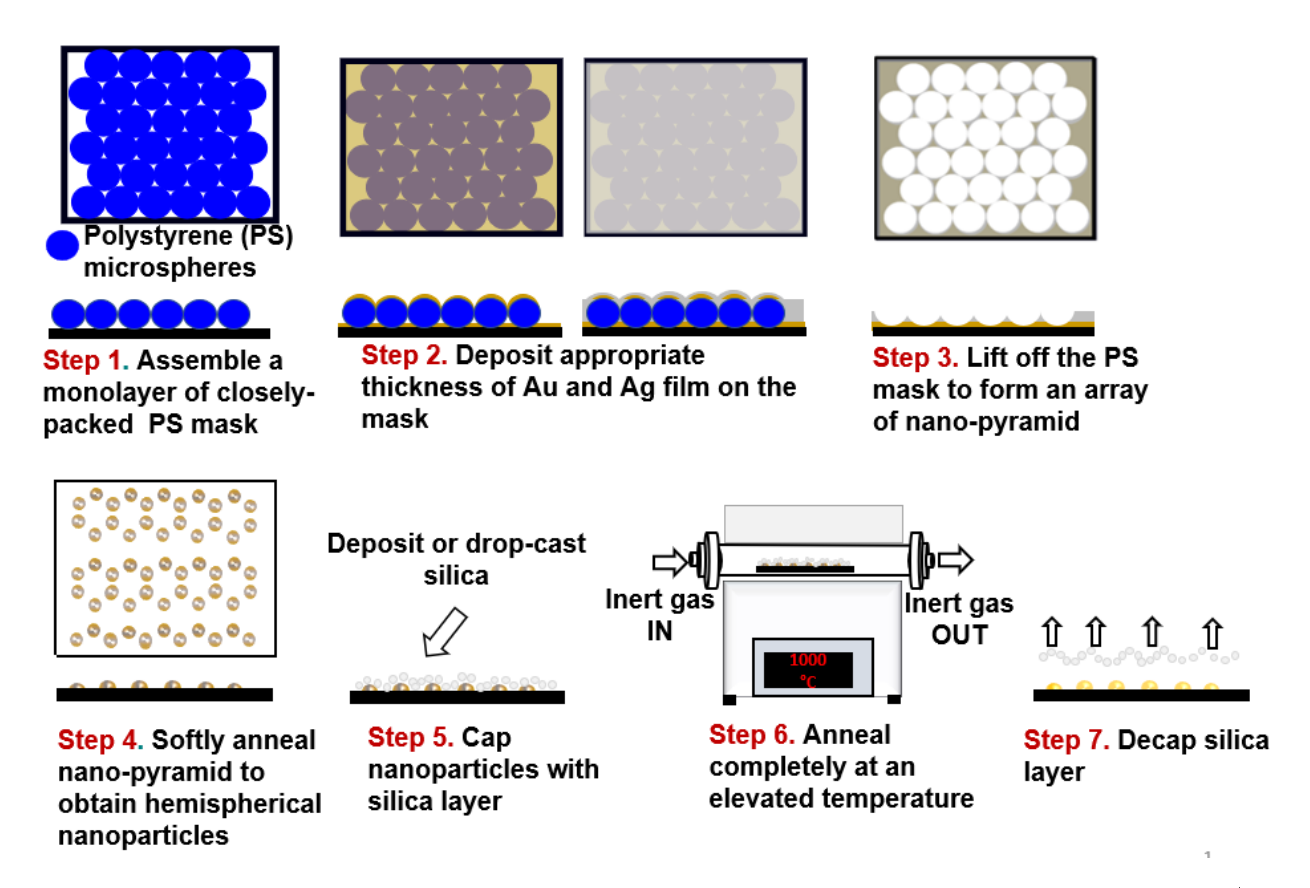


Figure 1: Schematic diagram of the step-wise procedure for fabricating fully alloyed Ag/Au hemispherical nanoparticle arrays.

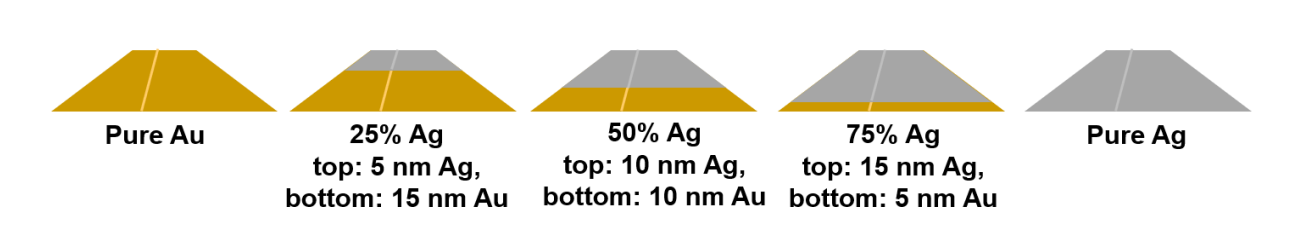


Figure 2: Schematic composition of pristine metals and single binary nano-pyramid following the deposition of Ag and Au films on the substrate (not to scale). Array of 25% Ag, 50% Ag, and 75% Ag are obtained by depositing 5 nm Ag over 15 nm Au, 10 nm Ag over 10 nm Au, 15 nm Ag over 5 nm Au, respectively.

## Fabrication of Ag/Au nano-pyramid array

The fabrication procedure is based on a method employed by our group previously in Ref. 10. The procedure is illustrated in Figure 1 and explained extensively in the supporting information. Briefly, a mask was assembled from 500 nm colloidal polystyrene microspheres (PS) on a clean fused silica substrate using a spin-coating technique (Figure S1). The PS mask formed a hexagonal close-packed homogeneous monolayer with an area of at least 2 by 2 mm. The substrate was cleaned prior to the assembly using thermal and chemical treatments. Subsequently, Ag and Au layers were sequentially deposited on the colloidal mask using a dual electron-beam evaporator. Ag/Au nanoparticles with 25% Ag, 50% Ag, and 75% Ag were fabricated by sequentially depositing 5 nm Ag film on 15 nm Au film, 10 nm Ag film on 10 nm Au film, 15 nm Ag film on 5 nm Au film, respectively. The effect of the pyramidal shape on the composition can be neglected since the lateral dimension of the pyramid is much larger than its height. Afterward, the colloidal microspheres were lifted off by ultrasonication in toluene, leaving behind a hexagonal pattern of triangular-based Ag/Au bimetallic nano-pyramids on the substrate (Figure 2). The substrate was rinsed with de-ionized water and dried under inert gas.

### Annealing, silica-capping and decapping

Low-temperature annealing of the Ag/Au nano-pyramid array at 400 °C is applied to convert the nanopyramids into hemispherical nanoparticles. As discussed below, without this step the nanoparticles remain in their pyramidal shape (Figure S2). Two silica-coating techniques were compared to cap the low-temperature annealed Ag/Au nanoparticles for protection before high-temperature annealing. High-temperature annealing was necessary to achieve complete alloying of the metals as discussed below. First, silica was synthesized using a sol-gel reaction of tetraethylorthosilicate with a tertiary amine (the procedure was adapted from ref 19 and is described in the supporting information). Secondly, silica was deposited on the low-temperature annealed Ag/Au nanoparticle array at a rate of 0.5 Å/sec, at 18° tilt

in a dual electron-beam evaporator. Slowly deposited silica by electron beam evaporation resulted in a compact silica coverage with little pore spaces. This method leads to better results as discussed below. The capped Ag/Au@SiO<sub>2</sub> nanoparticle arrays on the fused silica substrate were annealed at 1000 °C for 3 hours in an inert environment in a tube furnace. Following high-temperature annealing, the silica cap was removed in an alkaline solution of 0.1 M NaOH with about 100  $\mu$ L of diethylamine. Diethylamine was added to the alkaline solution to prevent the etching of the Ag component.

#### Synthesis of Cu<sub>2</sub>O semi-shell

Cu<sub>2</sub>O semi-shell was synthesized on the fully alloyed Ag/Au nanoparticle array after removing the silica coating using a CBD technique described previously. <sup>10</sup> Briefly, a chemical bath solution was prepared by adding 14 mL deionized (DI) water, 200  $\mu$ L of 0.1 M copper(II) sulfate pentahydrate solution (98%), 0.1 mL of 38.8 mM sodium citrate solution (100%) and 87 mg of sodium dodecyl sulfate (99%) into a beaker while stirring. The alloyed nanoparticle substrate was submerged in the chemical bath solution; subsequently, 250  $\mu$ L of 1 M sodium hydroxide solution (99%) and 100  $\mu$ L of 0.2 M hydroxylamine hydroxide (99%) were added dropwise. Thicker Cu<sub>2</sub>O semi-shells were obtained by increasing the growth time in the bath solution. Also, the concentration of copper(II) sulfate pentahydrate solution can be increased to synthesize thicker semi-shells. <sup>10</sup> Finally, the substrate was rinsed with DI water and dried under inert gas.

## RESULTS AND DISCUSSION

A series of fully alloyed Ag/Au nanoparticle arrays, with varying compositions of Ag and Au, were fabricated on fused silica and glass substrates for optical characterization and on silicon nitride grids for high-resolution transmission electron microscopy (HR-TEM) characterization. As illustrated in Figure 2, the composition of Ag and Au in the alloy array was

varied by changing the thickness of Ag and Au films deposited within a total film thickness of 20 nm. This approach was employed to maintain the size of the nanoparticle upon full alloying. It is important to note that the order of depositing the individual films, either as Ag/Au or Au/Ag, does not have an observable influence on the resulting alloys (Figure S3).<sup>3</sup> Due to the proximity of the lattice constants of Au and Ag (0.408 nm and 0.409 nm, respectively) it is very difficult to identify the individual components of the alloys. A combination of results from scanning electron microscopy - energy-dispersive X-ray spectroscopy (SEM-EDS), HR-TEM, X-ray diffraction (XRD) and X-ray photoelectron spectroscopy (XPS) has been employed to characterize the alloys.

# Characterization of Ag/Au nano-pyramid array

Figure 3 displays TEM images of Ag/Au nano-pyramids with different compositions of Ag and Au fabricated on a lacey carbon grid (Figure 3a-d) and on a silicon nitride grid (e,f) for HR-TEM. The individual nano-pyramids on lacey carbon were imaged with the PS mask in place after deposition of the metallic films before removal of the mask. This was necessary because the PS mask could not be lifted off of lacey carbon without removing the metals nanoparticles as well. The presence of the overlapping PS spheres can explain the apparent dark spots on the triangular structures (Figure 3c, top). Two different lattice fringe spacings were observed in HR-TEM (Figure 3d, magnification of the yellow square in (a)), 2.37 Å and 2.2 Å, which agree well with face-centered cubic (fcc) Ag (111) as well as Au (111). Variations of the fringe spacing can be explained by the imaging conditions due to the pyramidal shape and due to the composition change. Figure 3e and f show the nano-pyramid after PS sphere lift-off. Further investigation of the elemental composition of an individual nano-pyramid was conducted using SEM EDS displayed in Figure 4. The EDS spectra confirmed the presence of Ag and Au metals in the nano-pyramid's architecture after deposition and lift-off procedure, and before annealing.

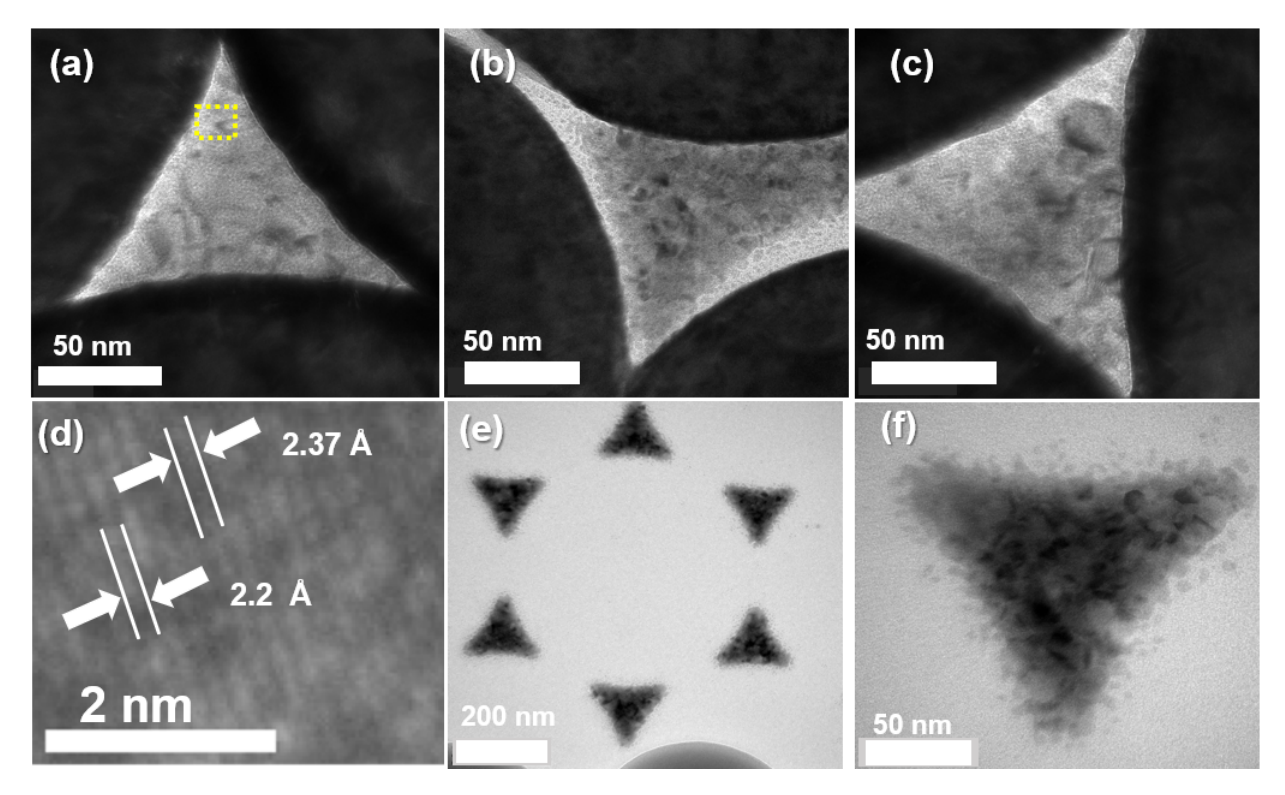


Figure 3: TEM images of individual Ag/Au binary alloy with (a) 25% Ag, (b) 50% Ag, (c) 75% Ag on lacey carbon grid before annealing. (d) HR-TEM image of Ag/Au alloy showing lattice fringes of fcc Ag (111) and Au (111) (magnification of the yellow square in (a)); (e-f) Ag/Au alloy on a silicon nitride grid.

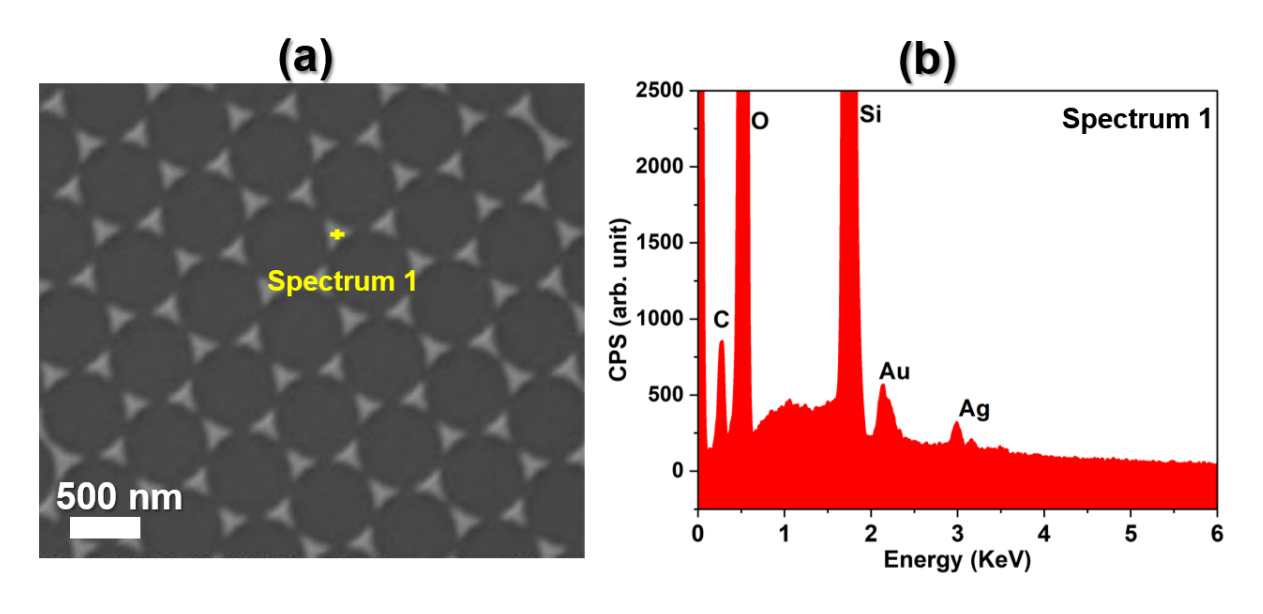


Figure 4: SEM-EDS results of Ag/Au nano-pyramid array (a) SEM image of Ag/Au nano-pyramid array with 25% Ag on a glass substrate (b) EDS spectra, taken at the position indicated in a), showing the presence of Ag and Au noble metals in the nano-pyramid.

## ${\bf Characterization\ of\ low-temperature\ annealed\ Ag/Au\ nano-pyramids}$

Two additional steps were incorporated before high-temperature annealing of the Ag/Au nano-pyramid array at 1000 °C. These processes include low-temperature annealing followed by capping with silica. A low-temperature annealing step was introduced to convert the nano-pyramid into hemispherical nanoparticles. Subsequent capping with silica is necessary to prevent the evaporation of Ag during high-temperature annealing. Low-temperature annealing at (400 °C) for 10 minutes was sufficient to convert the nano-pyramid into nearly hemispherical nanoparticles but did not result in fully alloyed particles. This process was conducted in an inert environment to prevent potential degradation or oxidation of Ag. It was observed that capping the nano-pyramids with silica without initial low-temperature annealing resulted in the nano-pyramids retaining their shape after high-temperature annealing (Figure S2). The shape-retention of the nano-pyramids during high-temperature annealing demonstrates the mechanical stability of the silica cap. TEM and SEM images of low-temperature annealed nanoparticles displayed in Figures 5 and S5, respectively, show that the annealing parameters are adequate to convert the nano-pyramids into nearly hemispherical nanoparticles. The dark spots that were observed around the nanoparticle in Figure 5a can be attributed to residue from the PS mask lift-off procedure on the silicon nitride TEM grid. The lift-off procedure was performed without a subsequent rinsing step to avoid washing off the alloy nanoparticles. These spots were not observed in SEM on fused silica or glass substrates after rinsing. Further investigation of elemental composition in the low-temperature annealed nanoparticles was conducted using TEM-EDS. The qualitative analysis of a low-temperature annealed nanoparticle with 25% Ag identify the presence of Au and Ag in the nanoparticles (Figure S6).

Following the low-temperature annealing of the Ag/Au nano-pyramid array, the hemispherical nanoparticles were capped with silica by CBD or by depositing ultrapure silica on the substrate with e-beam evaporation in an ultrahigh vacuum. E-beam deposition of silica resulted in a capping layer that could be removed without altering the nanoparticles.

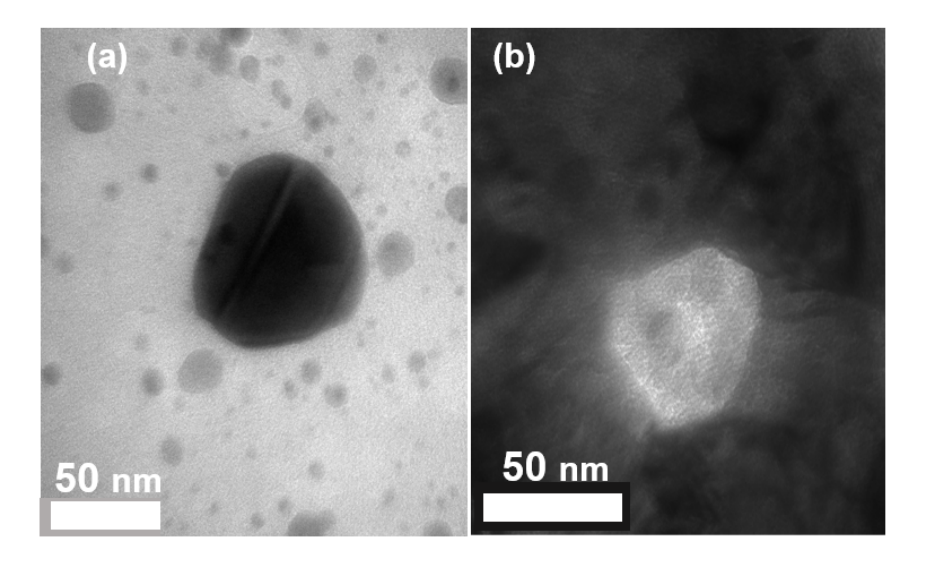


Figure 5: TEM images of (a) low-temperature annealed Ag/Au nanoparticle on silicon nitride grid (b) low-temperature annealed Ag/Au nanoparticle capped with silica. The dark spots surrounding the nanoparticle result from residues of the PS mask that are present because the silicon nitrite substrate did not allow subsequent rinsing.

Capping the nanoparticles using silica grown by CBD or drop-cast synthesis (the synthesis is described in the supporting information), on the other hand, resulted in a much denser silica layer after high-temperature annealing. The formation of this dense layer can be explained by silicate condensation.  $^{36}$  The resulting rigid silica shell is difficult to etch without destroying the alloys. Therefore, a layer of silica was deposited on the low-temperature annealed nanoparticle array by e-beam deposition in ultrahigh vacuum. The silica was deposited at a low rate of 0.5 Å/sec to reduce potential micropores in the silica cap.

## Characterization of fully alloyed ${\rm Ag/Au}$ nanoparticles

The morphological characterization of high-temperature annealed Ag/Au nanoparticle array was conducted on samples with varying compositions of Ag. The size difference before and after removal of the silica cap gives an estimate for the thickness of the silica cap of around 25 nm (size distributions in Figures S7 and S8). A representative SEM image of Ag/Au particles with 50% Ag composition after de-capping is displayed in Figure 6a. High-temperature annealing at a temperature of 1000 °C results in Ag/Au nanoparticle arrays that

differ from the initial low-temperature annealed ones. First, the shape of the nanoparticles became more spherical (Figure 6b). This can be attributed to some remaining flexibility of the silica cap at high temperatures and the strong cohesive force of the fully molten alloy. It should be noted that due to adhesion to the substrate the particles are hemispherical rather than perfectly spherical. The HR-TEM presented in Figure 6c (magnification of the yellow square in Figure 6b), shows uniform lattice spacing that lies in between the two lattice constants observed in the bimetallic nano-pyramids. <sup>44</sup> The uniform spacing and the absence of lattice mismatch indicate the formation of a highly crystalline homogeneous alloy. <sup>13,19</sup> In addition, fast Fourier transform (FFT) was conducted on the array in Figure 6a, to assess the order that was obtained. The hexagonal shape of the array's reciprocal lattice further supports that the alloy particles are well ordered on the substrate over large areas. As expected, NSL results in very homogeneous arrays of nanoparticles with very narrow size distributions (Figure S8). In addition, the alloys show very narrow FWHM of the LSPR of around 87 nm (Figure 7c).

The fact that the size is constant for particles with different Ag concentrations indicates that negligible amounts of silver were evaporated during the annealing steps (Figure S9). EDS elemental mapping has been employed for alloyed nanoparticles, however, it does not provide the required spatial resolution to convincingly show full alloying in the small nanoparticles presented here.

Optical characterization of the fully alloyed nanoparticles was conducted by UV-Vis spectroscopy. For comparison, pristine Au and Ag nanoparticle arrays of comparable sizes were fabricated on glass substrates (Figure S10). Figure 7b shows the well known LSPR for pure Au and Ag nanoparticles in black and purple. Pure Ag nanoparticles with a size of 80 nm show an LSPR at 516 nm while pure Au of about the same size show an LSPR at 590 nm.

Spectra of not fully alloyed, segregated Ag/Au particles have shown the presence of very broad plasmon bands, resembling the bands in Figure 7a, or bands comprising two peaks

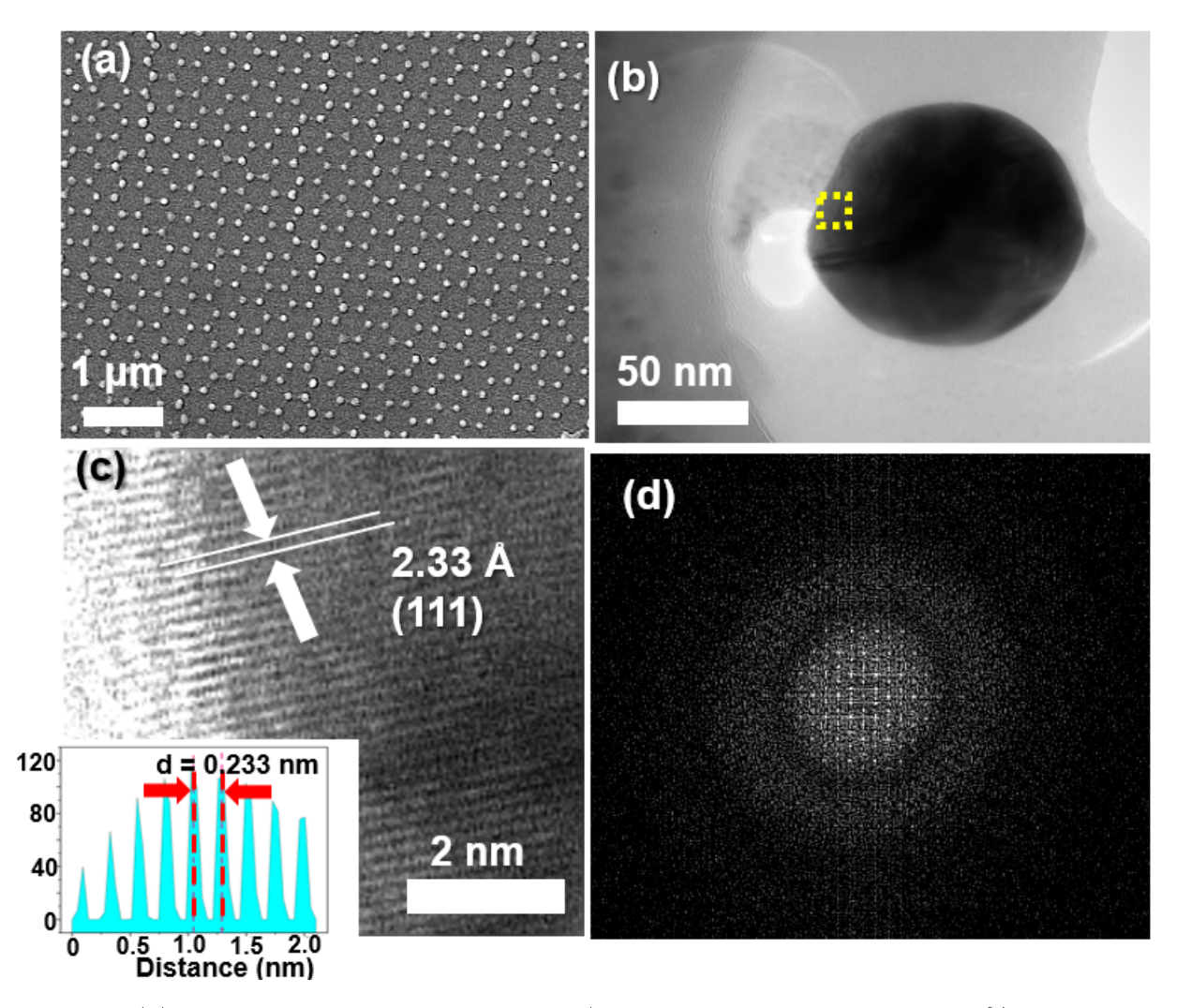


Figure 6: (a) SEM image of fully alloyed Ag/Au nanoparticle array with 75% Ag on fused silica substrate, (b)TEM image of a single Ag/Au nanoparticle with 50% Ag, (c) HR-TEM showing homogeneous crystalline lattice fringes of fully alloyed Ag/Au nanoparticle, Inset: profile of frame for the average width of the lattice fringe (d) Corresponding fast Fourier transformation of the periodic array in Figure 6a.

that correspond to the characteristic spectra of individual Ag and Au domains. <sup>14,16,19–21,45</sup> The broad plasmon bands can be attributed to a superposition of Ag and Au domains and to the damping of the surface plasmons induced by the presence of Ag/Au boundaries.

Figure 7b shows that fully alloyed Ag/Au nanoparticles exhibit a single, well-defined narrow LSPR that shifts linearly (Figure 7d) with composition between the LSPR of pristing Au and Ag nanoparticles of similar sizes. The absence of a broad or double-peak spectrum supports that full annealing of the Ag and Au components in the nanoparticle was achieved. The FWHM of the LSPR does only weakly dependent on the composition (Figure 7c). This can be expected, since major factors that govern the FWHM such as size and size distribution and the environment are identical for the different alloys. 46 The difference in plasmon dephasing time of Au and Ag has only a minor effect on the width of the LSPR. The optical properties of the alloy nanoparticles are in agreement with previous investigations, 13,17,19,30,45 and they confirm the possibility of tailoring the plasmonic property of Ag/Au alloys by varying the composition of the individual components. Defects such as stacking faults limit the size of the ordered arrays that can be achieved via the NSL technique.<sup>47</sup> However, Figure S1 clearly shows that several 10 x 10  $\mu$ m, defect free patches can be observed. The stacking faults have negligible effect on the plasmonic properties since individual nanoparticles are spaced far enough to prevent inter-particle interactions. A twist or shift of the hexagonal lattice at a stacking fault has no influence on the plasmonic properties as long as the particle size is preserved. This is confirmed by the narrow width and single, well-defined plasmon peak in UV-Vis.

### Ag/Au@Cu<sub>2</sub>O alloy/semiconductor nano-heterostructure array

For verification that the surface of the alloy particles is not significantly modified by the capping/de-capping procedure, Cu<sub>2</sub>O semi-shell was added to the de-capped alloy nanoparticles. The method for the synthesis of the Cu<sub>2</sub>O semi-shell utilizes the nanoparticles as seeds to guide the growth of the Cu<sub>2</sub>O shell while providing control over their morphology

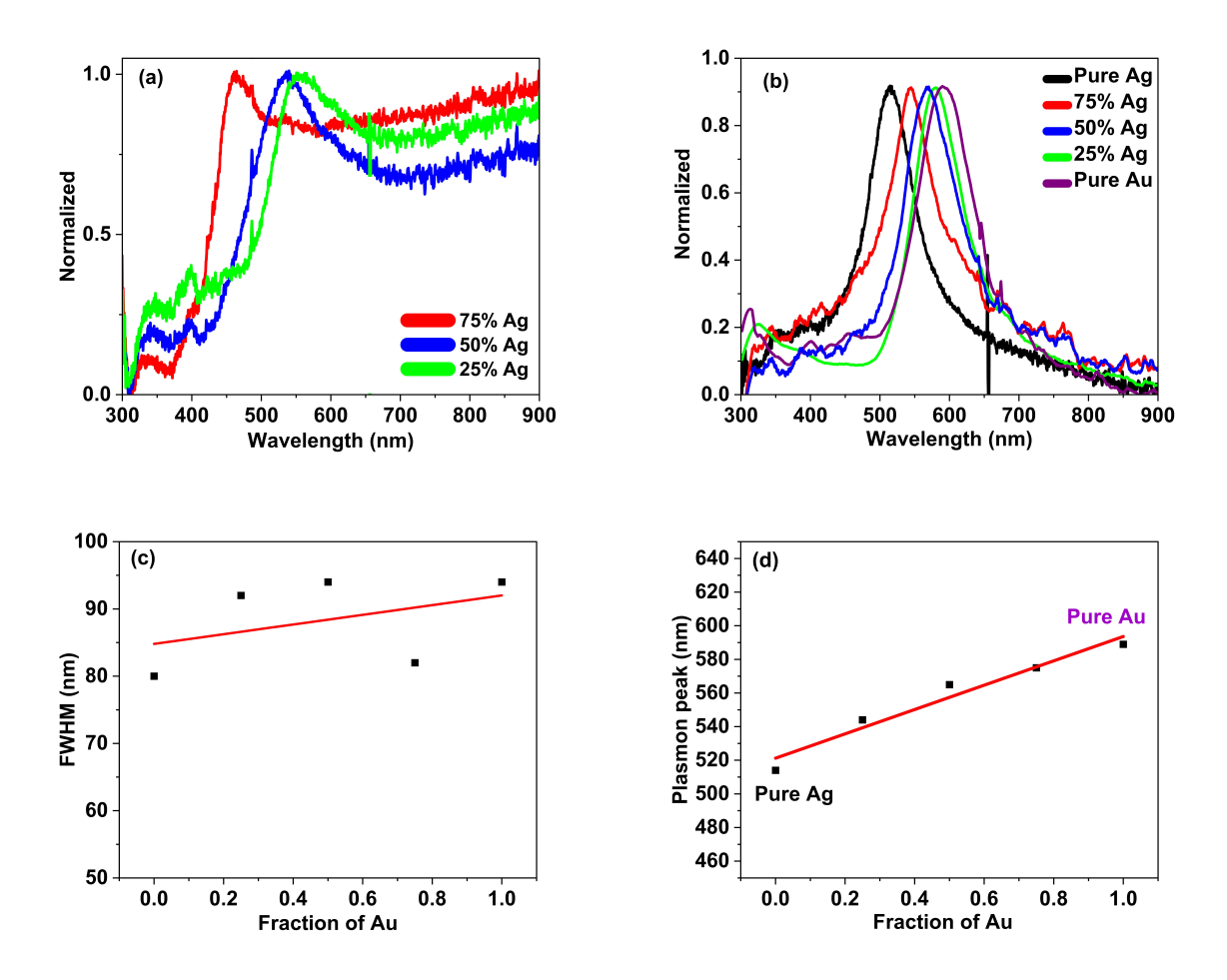


Figure 7: UV-Vis absorption spectra of the plasmon peaks. Spectra of (a) low-temperature annealed alloys; (b) pure Ag, and Au nanoparticles, and high-temperature annealed alloys; (c-d) linear variation of full width at half maximum (FWHM) and plasmon peak maxima with increasing Au fraction.

and thickness.<sup>10</sup> The thickness of the nanocrystalline Cu<sub>2</sub>O semi-shell is varied by controlling the reaction time and precursor concentration. Figures 8(a-d) show TEM images of Cu<sub>2</sub>O coated nanoparticles with varying thicknesses of ~10 nm, ~15 nm, and ~20 nm grown on a Ag/Au alloy nanoparticle. In addition, Figure S4 shows an Ag/Au@Cu<sub>2</sub>O nanoparticle that was scraped off of the substrate and placed on the side on a TEM grid. The image clearly shows the morphology of the hemispherical core and the Cu<sub>2</sub>O semi-shell. The lattice fringes observed in the HR-TEM image show an interplanar spacing of 2.42 Å which corresponds to Cu<sub>2</sub>O with a fcc structure in the (111) plane. It should be noted that the homogeneous coverage of the alloy with Cu<sub>2</sub>O strongly indicates that the silica capping layer was completely removed during etching since Cu<sub>2</sub>O does not form on fused silica or silicon nitrite under these growth conditions.

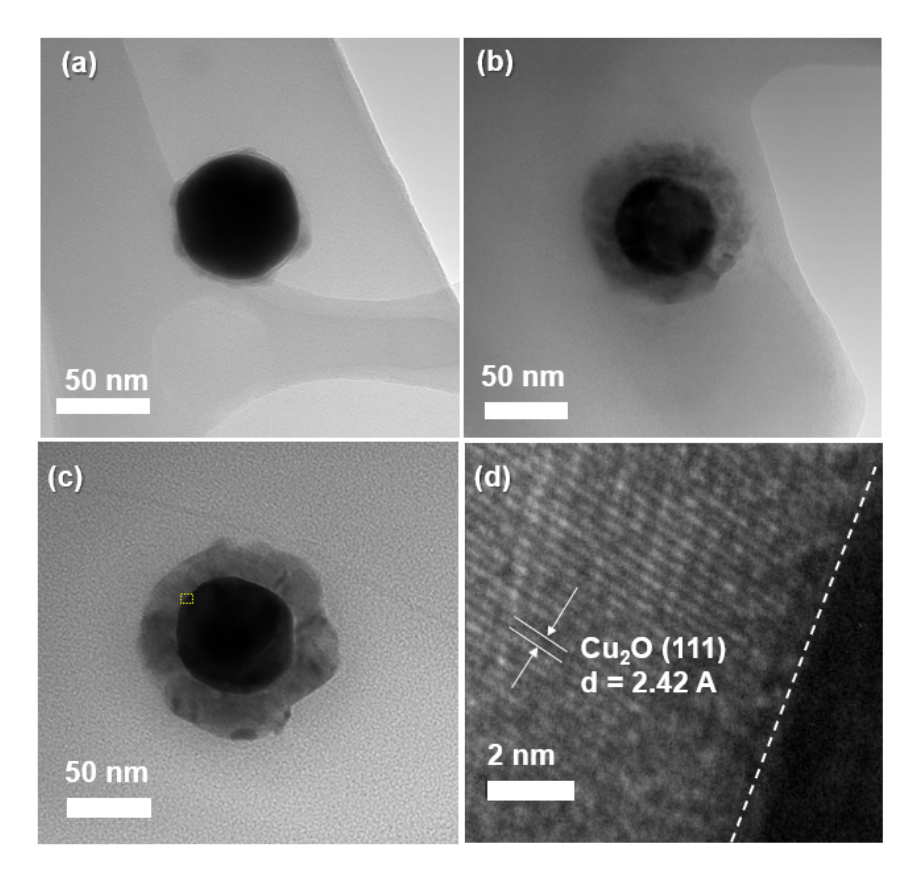


Figure 8: TEM images of fully alloyed 50:50 Ag/Au with increasing sizes of  $Cu_2O$  semi-conductor shell (a)  $\sim 10$  nm (b)  $\sim 15$  nm (c)  $\sim 20$  nm (d) HR-TEM image of the interface between alloy and  $Cu_2O$ .

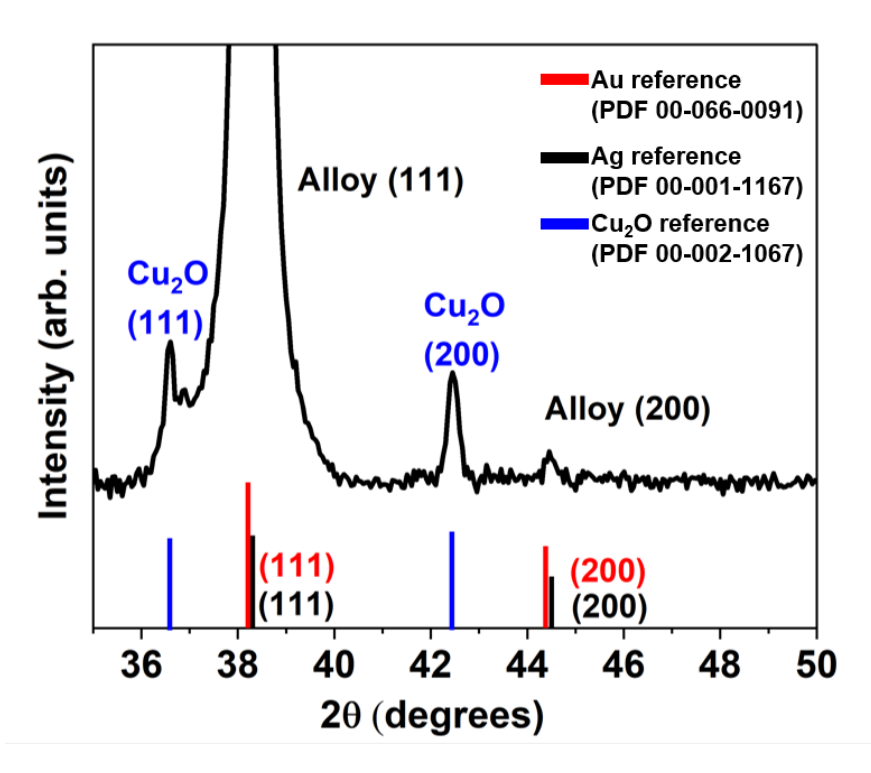


Figure 9: Expanded XRD pattern of Ag/Au@Cu<sub>2</sub>O heterostructure showing Au (PDF 00-066-0091, red), Ag(PDF 00-001-1167, black) and Cu<sub>2</sub>O (PDF 00-002-1067, blue).

Characterization of the crystal structure and elemental composition were conducted using XRD (Figure 9) and XPS (Figure 10). The XRD pattern of Ag/Au@Cu<sub>2</sub>O nanoheterostructure shows peaks corresponding to fcc (111) and (200) planes for the alloy and semiconductor. The prominent peak at 38.25° agrees very well with the references for the (111) plane of fcc Au (red bar in Fig. 9, PDF 00-066-0091) as well as Ag (black bar in Fig. 9, PDF 00-001-1167) at 38.2° and 38.33°, respectively. This would agree with the expected value for a fully alloyed solid solution. However, the peaks for Au and Ag are too close together to distinguish an alloy from a composite by XRD. The same holds true for the peak at 44.45° that agrees well with the reference for the (200) plane of Au and Ag at 44.39° as well as 44.5°, respectively. In addition, the smaller peaks at 36.58° and 42.43° correspond to (111) and (200) planes of fcc Cu<sub>2</sub>O (PDF 00-002-1067), respectively. This result suggests that the preferred orientation planes for Ag/Au alloy are (111) and (200) orientation. This can be attributed to the two annealing procedures during fabrication. <sup>10</sup> However, the diffrac-

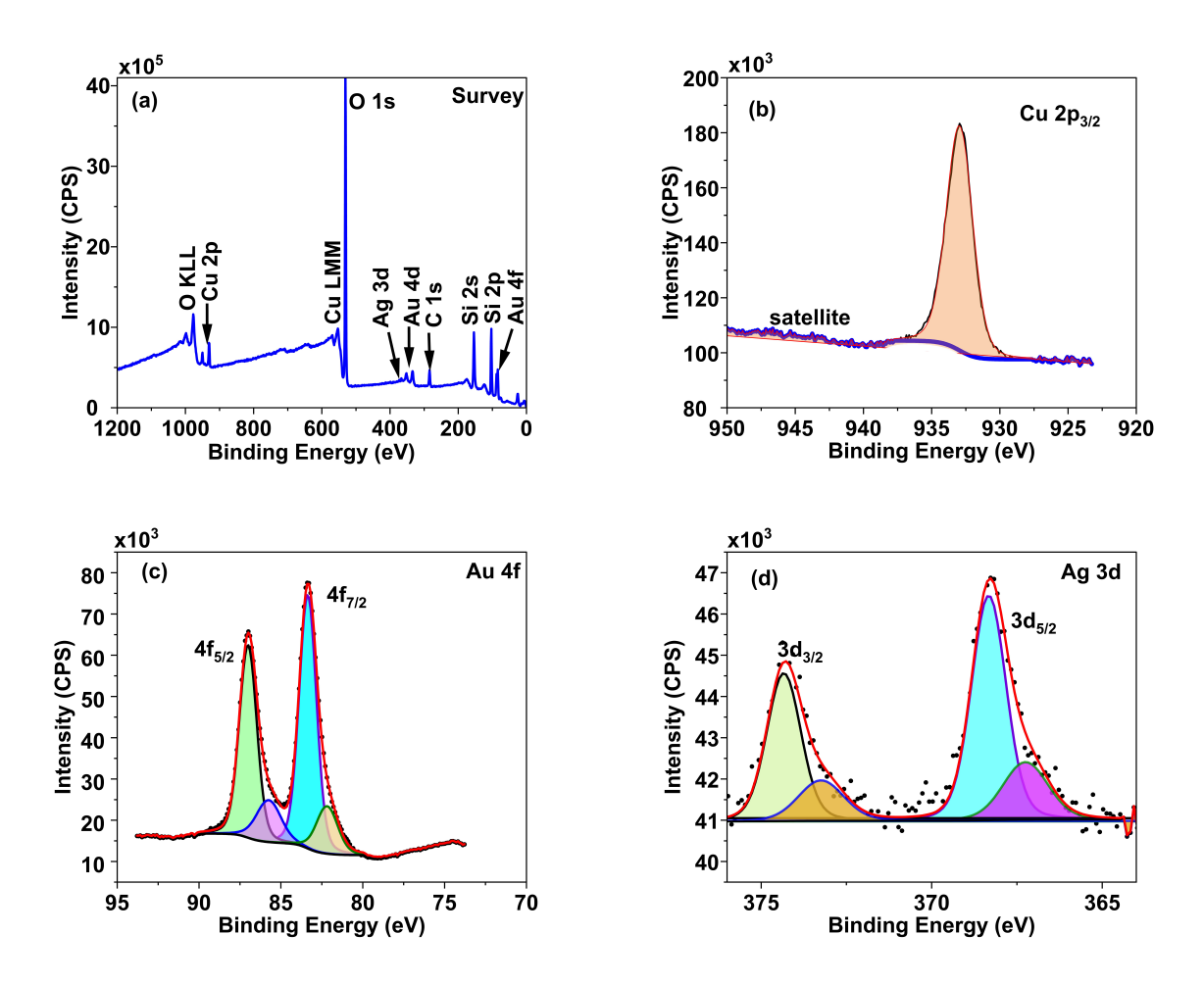


Figure 10: XPS result of Ag/Au@Cu<sub>2</sub>O heterostructure (a) survey spectrum (b) Cu  $2p_{3/2}$  (c) Au 4f (d) Ag 3d.

tion intensity of the (111) plane is much stronger compared to the (200) plane for Au, Ag, and Cu<sub>2</sub>O, which indicates that the preferred orientation plane is (111). This shows that the synthetic method presented here results in homogeneous morphology and crystal orientation of Cu<sub>2</sub>O with respect to the alloy seeding template. The XPS survey spectrum in Figure 10a show peaks that can be attributed to the presence of Ag/Au alloy, Cu<sub>2</sub>O semiconductor, and the fused silica substrate. The peaks can be assigned to Ag 3d, Au 3d, Au 4f, Cu 2p, and Cu LMM (Auger). Further analyses of the high-resolution core-level XPS spectrum presented in Figure 10(b-d) clearly shows the presence of a well-resolved Cu 2p<sub>3/2</sub>, Au 4f doublet (7/2 and 5/2 spins) and Ag 3d doublet (5/2 and 3/2 spins). The Cu  $2\mathrm{p}_{3/2}$  spectrum displays a prominent peak at 933 eV and a very weak satellite around 945 eV. This feature confirms the presence of Cu<sup>+</sup> in Cu<sub>2</sub>O.<sup>10</sup> Secondly, the Au 4f spectrum shows the presence of a well-resolved metallic (Au<sup>0</sup>) doublet with 7/2 and 5/2 spins, with 3.67eV splitting. <sup>10</sup> However, the presence of small amounts of Au<sup>+</sup> was observed in the spectra. These components can be attributed to impurities introduced after fabrication. Finally, the Ag 3d spectrum displays the presence of 3d doublet at 368.2 eV (FWHM = 1.2 eV) and 374.2 ev (FWHM = 1.2 eV), with a 6 eV splitting. This result is in good agreement with the presence of metallic silver Ag<sup>0</sup>. 48 Small amounts of cationic silver were observed in the data, similar to what was observed in Au. However, the XRD data does not show any peak at 46.17° that would indicate the presence of significant amounts of Ag<sub>2</sub>O (132).<sup>49</sup> Hence, it is assigned to oxidation accumulated on the sample after fabrication. The presence of predominantly metallic Ag in the fully alloyed nanoparticles after high-temperature annealing at an elevated temperature of 1000°C and etching in an alkaline environment proves the effectiveness of this strategy in protecting the Ag component of the alloy. The growth characteristic and the properties of the Cu<sub>2</sub>O semi-shell are identical to those of semi-shells grown on pure gold nanoparticles that did not undergo a capping / de-capping procedure. <sup>10</sup> This shows that the silica cap was completely removed without major alterations to the surface. The alloy's surface is therefore accessible to functionalization by molecules, polymers, or semiconductors. Such composites, could be instrumental for understanding plasmon/exciton coupling and other fundamental processes. The possible applications range from solar energy conversion, photocatalysis, photodetection, and photovoltaics.

### Conclusion

We demonstrated a flexible method for the fabrication of regular arrays of fully alloyed Ag/Au nanoparticles based on NSL and PVD. A low-temperature annealing step resulted in nearly spherical particles that were protected by a silica cap during high-temperature annealing. The silica cap that was applied via e-beam evaporation provided enough flexibility to allow the particles to acquire a near perfect spherical shape. At the same time it could be removed via etching under mild conditions without affecting the alloy nanoparticles. Complete removal and accessibility of the alloy surface after etching was demonstrated by functionalizing the nanoparticles with a Cu<sub>2</sub>O shell. The resulting nano-heterostructure could serve as hybrid plasmonic materials for converting and harvesting plasmonic excitations with promising potentials for photocatalysis, energy conversion and storage.

The approach presented here can be applied for different PVD-based methods beyond NSL including soft lithography involving self-assembly monolayers, block co-polymers, and aggregated mesoscale objects. Since the protective coating preserves composition during high temperature annealing, higher alloys and even doping with trace elements can be achieved by co-deposition, depending on their compatibility with PVD.

## **Supporting Information**

Fabrication and characterization details, SEM and TEM images, UV-vis spectra.

## Acknowledgement

This material is based upon work supported by the Division of Materials Research (DMR), National Science Foundation under Grant No. 2116514. This research was partially supported by NSF through the University of Delaware Materials Research Science and Engineering Center DMR-2011824. XPS analysis was performed with the instrument sponsored by the National Science Foundation under grant No. CHE-1428149. We acknowledge the support provided by Professor Chaoying Ni, and Dr. Yong Zhao at the W.M Keck Center for Advanced Microscopy and Microanalysis (Keck CAMM), University of Delaware. Also, we thank Gerald Poirier and Dr. Jing Qu in the Advanced Materials Characterization Lab (AMCL) at the University of Delaware for their technical support during XRD measurement.

### References

- (1) Zhang, H.; Cadusch, J.; Kinnear, C.; James, T.; Roberts, A.; Mulvaney, P. Direct Assembly of Large Area Nanoparticle Arrays. ACS Nano 2018, 12, 7529-7537.
- (2) Kuemin, C.; Stutz, R.; Spencer, N. D.; Wolf, H. Precise Placement of Gold Nanorods by Capillary Assembly. *Langmuir* 2011, 27, 6305–6310.
- (3) Kozioł, R.; Łapiński, M.; Syty, P.; Sadowski, W.; Sienkiewicz, J. E.; Nurek, B.; Maraloiu, V. A.; Kościelska, B. Experimental tuning of AuAg nanoalloy plasmon resonances assisted by machine learning method. *Applied Surface Science* **2021**, *567*, 150802.
- (4) Wu, K.; Lian, T. Quantum confined colloidal nanorod heterostructures for solar-to-fuel conversion. *Chemical Society Reviews* **2016**, *45*, 3781–3810.
- (5) Sobhani, A.; Knight, M. W.; Wang, Y.; Zheng, B.; King, N. S.; Brown, L. V.; Fang, Z.; Nordlander, P.; Halas, N. J. Narrowband photodetection in the near-infrared with a plasmon-induced hot electron device. *Nature Communications* **2013**, 4.

- (6) Le, F.; Brandl, D. W.; Urzhumov, Y. A.; Wang, H.; Kundu, J.; Halas, N. J.; Aizpurua, J.; Nordlander, P. Metallic Nanoparticle Arrays: A Common Substrate for Both Surface-Enhanced Raman Scattering and Surface-Enhanced Infrared Absorption. ACS Nano 2008, 2, 707–718.
- (7) Lin, J.; Wang, S.; Huang, P.; Wang, Z.; Chen, S.; Niu, G.; Li, W.; He, J.; Cui, D.; Lu, G.; Chen, X.; Nie, Z. Photosensitizer-Loaded Gold Vesicles with Strong Plasmonic Coupling Effect for Imaging-Guided Photothermal/Photodynamic Therapy. ACS Nano 2013, 7, 5320–5329.
- (8) Zheng, B. Y.; Zhao, H.; Manjavacas, A.; McClain, M.; Nordlander, P.; Halas, N. J. Distinguishing between plasmon-induced and photoexcited carriers in a device geometry.

  Nature Communications 2015, 6.
- (9) Jiang, R.; Li, B.; Fang, C.; Wang, J. Metal/Semiconductor Hybrid Nanostructures for Plasmon-Enhanced Applications. *Advanced Materials* **2014**, *26*, 5274–5309.
- (10) Jia, M.; Zhang, Y.; Li, Z.; Crouch, E.; Doble, S.; Avenoso, J.; Yan, H.; Ni, C.; Gundlach, L. A versatile strategy for controlled assembly of plasmonic metal/semiconductor hemispherical nano-heterostructure arrays. *Nanoscale* **2020**, *12*, 17530–17537.
- (11) Gao, C.; Lu, Z.; Liu, Y.; Zhang, Q.; Chi, M.; Cheng, Q.; Yin, Y. Highly Stable Silver Nanoplates for Surface Plasmon Resonance Biosensing. *Angewandte Chemie International Edition* **2012**, *51*, 5629–5633.
- (12) Nishijima, Y.; Akiyama, S. Unusual optical properties of the Au/Ag alloy at the matching mole fraction. *Optical Materials Express* **2012**, *2*, 1226.
- (13) Rodríguez-González, B.; Sánchez-Iglesias, A.; Giersig, M.; Liz-Marzán, L. M. AuAg bimetallic nanoparticles: formation, silica-coating and selective etching. Faraday Discuss. 2004, 125, 133–144.

- (14) Link, S.; Wang, Z. L.; El-Sayed, M. A. Alloy Formation of Gold-Silver Nanoparticles and the Dependence of the Plasmon Absorption on Their Composition. *The Journal of Physical Chemistry B* 1999, 103, 3529–3533.
- (15) Gao, C.; Zhang, Q.; Lu, Z.; Yin, Y. Templated Synthesis of Metal Nanorods in Silica Nanotubes. *Journal of the American Chemical Society* **2011**, *133*, 19706–19709.
- (16) Hubenthal, F.; Borg, N.; Träger, F. Optical properties and ultrafast electron dynamics in gold-silver alloy and core-shell nanoparticles. *Applied Physics B* **2008**, *93*, 39–45.
- (17) Rioux, D.; Meunier, M. Seeded Growth Synthesis of Composition and Size-Controlled Gold-Silver Alloy Nanoparticles. The Journal of Physical Chemistry C 2015, 119, 13160-13168.
- (18) Zaleska-Medynska, A.; Marchelek, M.; Diak, M.; Grabowska, E. Noble metal-based bimetallic nanoparticles: the effect of the structure on the optical, catalytic and photocatalytic properties. *Advances in Colloid and Interface Science* **2016**, *229*, 80–107.
- (19) Gao, C.; Hu, Y.; Wang, M.; Chi, M.; Yin, Y. Fully Alloyed Ag/Au Nanospheres: Combining the Plasmonic Property of Ag with the Stability of Au. *Journal of the American Chemical Society* **2014**, *136*, 7474–7479.
- (20) ichi Naya, S.; Fujishima, M.; Tada, H. Synthesis of Au–Ag Alloy Nanoparticle-Incorporated AgBr Crystals. *Catalysts* **2019**, *9*, 745.
- (21) Guisbiers, G.; Mendoza-Cruz, R.; Bazán-Díaz, L.; Velázquez-Salazar, J. J.; Mendoza-Perez, R.; Robledo-Torres, J. A.; Rodriguez-Lopez, J.-L.; Montejano-Carrizales, J. M.; Whetten, R. L.; José-Yacamán, M. Electrum, the Gold-Silver Alloy, from the Bulk Scale to the Nanoscale: Synthesis, Properties, and Segregation Rules. ACS Nano 2015, 10, 188–198.

- (22) Csapó, E.; Oszkó, A.; Varga, E.; Juhász, Á.; Buzás, N.; Kőrösi, L.; Majzik, A.; Dékány, I. Synthesis and characterization of Ag/Au alloy and core(Ag)-shell(Au) nanoparticles. Colloids and Surfaces A: Physicochemical and Engineering Aspects 2012, 415, 281–287.
- (23) Cerbelaud, M.; Ferrando, R.; Barcaro, G.; Fortunelli, A. Optimization of chemical ordering in AgAu nanoalloys. *Physical Chemistry Chemical Physics* **2011**, *13*, 10232.
- (24) van der Hoeven, J. E. S.; Welling, T. A. J.; Silva, T. A. G.; van den Reijen, J. E.; Fontaine, C. L.; Carrier, X.; Louis, C.; van Blaaderen, A.; de Jongh, P. E. In Situ Observation of Atomic Redistribution in Alloying Gold-Silver Nanorods. ACS Nano 2018, 12, 8467-8476.
- (25) Yang, C. C.; Mai, Y.-W. Thermodynamics at the nanoscale: A new approach to the investigation of unique physicochemical properties of nanomaterials. *Materials Science and Engineering: R: Reports* **2014**, *79*, 1–40.
- (26) Guisbiers, G.; Mejia-Rosales, S.; Khanal, S.; Ruiz-Zepeda, F.; Whetten, R. L.; José-Yacaman, M. Gold-Copper Nano-Alloy, Tumbaga, in the Era of Nano: Phase Diagram and Segregation. Nano Letters 2014, 14, 6718-6726.
- (27) Delfour, L.; Creuze, J.; Legrand, B. Exotic Behavior of the Outer Shell of Bimetallic Nanoalloys. *Physical Review Letters* **2009**, *103*, 205701.
- (28) Yu, H.; Peng, Y.; Yang, Y.; Li, Z.-Y. Plasmon-enhanced light-matter interactions and applications. npj Computational Materials 2019, 5.
- (29) yakout El koraychy, E.; Nelli, D.; Roncaglia, C.; Minnai, C.; Ferrando, R. Growth of size-matched nanoalloys a comparison of AuAg and PtPd. *The European Physical Journal Applied Physics* **2022**, *97*, 28.

- (30) Cortie, M. B.; McDonagh, A. M. Synthesis and Optical Properties of Hybrid and Alloy Plasmonic Nanoparticles. *Chemical Reviews* **2011**, *111*, 3713–3735.
- (31) Gonzalez, C. M.; Liu, Y.; Scaiano, J. C. Photochemical Strategies for the Facile Synthesis of Gold-Silver Alloy and Core-Shell Bimetallic Nanoparticles. *The Journal of Physical Chemistry C* **2009**, *113*, 11861–11867.
- (32) Besner, S.; Meunier, M. Femtosecond Laser Synthesis of AuAg Nanoalloys: Photoin-duced Oxidation and Ions Release. *The Journal of Physical Chemistry C* **2010**, *114*, 10403–10409.
- (33) Peng, Z.; Spliethoff, B.; Tesche, B.; Walther, T.; Kleinermanns, K. Laser-Assisted Synthesis of Au-Ag Alloy Nanoparticles in Solution. *The Journal of Physical Chemistry B* **2006**, *110*, 2549–2554.
- (34) Grade, S.; Eberhard, J.; Jakobi, J.; Winkel, A.; Stiesch, M.; Barcikowski, S. Alloying colloidal silver nanoparticles with gold disproportionally controls antibacterial and toxic effects. *Gold Bulletin* **2013**, *47*, 83–93.
- (35) Srinoi, P.; Chen, Y.-T.; Vittur, V.; Marquez, M.; Lee, T. Bimetallic Nanoparticles: Enhanced Magnetic and Optical Properties for Emerging Biological Applications. *Applied Sciences* **2018**, *8*, 1106.
- (36) Liu, K.; Bai, Y.; Zhang, L.; Yang, Z.; Fan, Q.; Zheng, H.; Yin, Y.; Gao, C. Porous Au–Ag Nanospheres with High-Density and Highly Accessible Hotspots for SERS Analysis. *Nano Letters* **2016**, *16*, 3675–3681.
- (37) Jensen, T. R.; Malinsky, M. D.; Haynes, C. L.; Van Duyne, R. P. Nanosphere Lithography: Tunable Localized Surface Plasmon Resonance Spectra of Silver Nanoparticles. The Journal of Physical Chemistry B 2000, 104, 10549–10556.

- (38) Haynes, C. L.; Duyne, R. P. V. Nanosphere Lithography: A Versatile Nanofabrication Tool for Studies of Size-Dependent Nanoparticle Optics. *The Journal of Physical Chemistry B* **2001**, *105*, 5599–5611.
- (39) Colson, P.; Henrist, C.; Cloots, R. Nanosphere Lithography: A Powerful Method for the Controlled Manufacturing of Nanomaterials. *Journal of Nanomaterials* **2013**, *2013*, 1–19.
- (40) Zhang, G.; Wang, D.; Möhwald, H. Ordered Binary Arrays of Au Nanoparticles Derived from Colloidal Lithography. *Nano Letters* **2006**, 7, 127–132.
- (41) Wang, W.; Ma, Y.; Qi, L. High-Performance Photodetectors Based on Organometal Halide Perovskite Nanonets. *Advanced Functional Materials* **2017**, *27*, 1603653.
- (42) Liang, X.; Dong, R.; Ho, J. C. Self-Assembly of Colloidal Spheres toward Fabrication of Hierarchical and Periodic Nanostructures for Technological Applications. *Advanced Materials Technologies* **2019**, 4, 1800541.
- (43) Ingram, W.; Larson, S.; Carlson, D.; Zhao, Y. Ag-Cu mixed phase plasmonic nanostructures fabricated by shadow nanosphere lithography and glancing angle co-deposition.

  Nanotechnology 2016, 28, 015301.
- (44) Long, V. C.; Quoc, V. D.; Trong, D. N. Ab Initio Calculations on the Structural and Electronic Properties of AgAu Alloys. *ACS Omega* **2020**, *5*, 31391–31397.
- (45) Agrawal, V. V.; Mahalakshmi, P.; Kulkarni, G. U.; Rao, C. N. R. Nanocrystalline Films of Au-Ag, Au-Cu, and Au-Ag-Cu Alloys Formed at the Organic-Aqueous Interface. *Langmuir* 2005, 22, 1846–1851.
- (46) Voisin, C.; Fatti, N. D.; Christofilos, D.; Vallée, F. Ultrafast Electron Dynamics and Optical Nonlinearities in Metal Nanoparticles. 105, 2264–2280.

- (47) Gates, B. D.; Xu, Q.; Stewart, M.; Ryan, D.; Willson, C. G.; Whitesides, G. M. New Approaches to Nanofabrication: Molding, Printing, and Other Techniques. 105, 1171–1196.
- (48) Firet, N. J.; Blommaert, M. A.; Burdyny, T.; Venugopal, A.; Bohra, D.; Longo, A.; Smith, W. A. Operando EXAFS study reveals presence of oxygen in oxide-derived silver catalysts for electrochemical CO<sub>2</sub> reduction. *Journal of Materials Chemistry A* 2019, 7, 2597–2607.
- (49) Yang, Q.; Li, D.; Yu, B.; Huang, S.; Wang, J.; Li, S.; Kang, J. Size Effect on Morphology and Optical Properties of Branched ZnO/Si nanowire arrays. *PHYSICS LETTERS A* **2016**, *380*, 1044–1048.